Stochastically Based Wet Snow Detection with Multitemporal SAR Data

Nikola Besic, Gabriel Vasile, Jocelyn Chanussot, Srdjan Stankovic, Jean-Pierre Dedieu

Stochastically Based Wet Snow Detection with Multitemporal SAR Data

Nikola Besic[(1),(2)], Gabriel Vasile[(1)], Jocelyn Chanussot[(1)], Srdjan Stankovic[(2)], Jean-Pierre Dedieu[(3)]

[(1)]: Grenoble-Image-sPeech-Signal-Automatics Lab
GIPSA-lab, CNRS / Grenoble INP - BP 46, 38402 Saint Martin D'Heres Cedex, France
Tel: +33 (0)4 76 57 45 75 - Fax: +33 (0)4 76 57 47 90 - Email : nikola.besic@gipsa-lab.grenoble-inp.fr

[(2)]: Electrical Engineering Department, University of Montenegro
ETF, UCG - Dzordza Vasingtona bb. 81000, Podgorica, Montenegro
Tel: +382 (20) 245 839 - Fax: +382 (20) 245 873 - Email: srdjan@ac.me

[(3)]: Laboratory for the study of Transfers in Hydrology and Environment
LTHE, CNRS / UJF - BP 53, 38041 Grenoble Cedex 09, France
Tel: +33 (0)4 56 52 09 77 - Fax: +33 (0)4 76 63 58 87 - Email: jean-pierre.dedieu@ujf-grenoble.fr

ABSTRACT

This paper proposes a new method for wet snow detection using multitemporal SAR data. The proposed change detection method is primarily based on the comparison between two X band SAR images acquired during the accumulation (winter) and the melting (spring) seasons, in the French Alps. The new membership decision method is relying on the local intensity statistics of the SAR images by considering the backscattering ratio as a stochastic process: the probability that "the intensity ratio is smaller than the corresponding locally varying dry/wet snow threshold" is larger than a predefined confidence level. The proposed snow backscattering simulations indicate a far more complex relation between the backscattering properties of the two snow types, with respect to the conventional assumption of the augmented electromagnetic absorption associated to the wet snow. The most conclusive results are confirmed at X band by *in situ* measurements. We show that this complexity is mostly caused by the dominance of a different backscattering component for each type of snow, leading to a significant angular sensitivity. Therefore, we introduce a variable threshold matrix instead of an unique threshold: the threshold is expressed as a function of the local incidence angle (LIA) for each pixel. The proposed snow backscattering simulator (SBS) allows deriving the locally varying threshold as the ratio between dry and wet snow backscattering coefficients computed for the SAR system parameters (polarization, frequency), the local topography parameters (LIA) and for the *a priori* derived and spatially averaged target parameters (underlying ground and snow cover surface properties, snow grain size, underlying ground dielectric permittivity, snow wetness). The threshold varying with respect to the frequency and the choice of the winter season reference image, allow the proposed algorithm applicability in wider frequency range.

I. INTRODUCTION

Snow cover represents a significant water resource in mountainous regions such as the French Alpes. The exact amount of liquid water contained in the snow pack is given through the physical quantity - Snow Water Equivalent (SWE). Due to numerous difficulties in performing "in situ" measurements (high altitudes, global coverage), the estimation of this quantity

turns out to be suitable for remote sensing applications. Generally, the SWE is a function of two independent snow physical properties: density and depth [1]. The significant snow pack penetration, along with the high spatial resolution and the clouds penetration capability, candidates Synthetic Aperture Radar (SAR) remote sensing for this kind of application [2], [3].

Depending on the liquid water content, snow can be considered as dry or wet. Dry snow is defined as snow consisted just of ice crystals embedded in air, without any liquid water. Its presence is characteristic for temperatures below $0°$C. Wet snow can be found during the melting season, when the temperature exceeds $0°$C. It contains a certain amount of liquid water introduced quantitatively through the wetness (volumetric liquid water content) [4]. These two snow types behave like two completely different materials with respect to their dielectric properties: the wet snow contains liquid water with a dielectric constant differing significantly from the one of the ice. This fact is pointing out to a difference in backscattering mechanisms [5], and consequently that different feature extraction methods should be applied. Therefore, the estimation of any snow pack parameter defining the SWE, by means of SAR remote sensing, requires firstly the proper identification of the snow cover type.

Although studies on snow mapping by polarimetric SAR existed already [6], it was not before the ERS-1 started providing repeat pass images that the idea of snow mapping based on SAR multitemporal data appeared [7]. Further refinement on the initial change detection method leaded eventually to the compact algorithm based on the ratio of two C band SAR images introduced in [8]. The Nagler and Rott method requires as inputs the SAR wet snow image and the reference SAR image of the dry snow (or the snow free terrain). After corregistration, either mutilooking or speckle filtering is applied on the two SAR intensities before constructing the backscattering ratio image. This ratio image is then georeferenced and an unique threshold of -3 dB is used to discriminate the wet snow from other surfaces. The expected difference in backscattering is justified by the increased electromagnetic absorption of the wet snow. The resulting maps are successfully validated by using snow terrain optical images.

We propose in this article a novel snow change detection method with X-band SAR data for wet snow detection [9]. Our goal is to introduce an algorithm which can be applied to a wider frequency range and is eventually more suited to the presence of the speckle noise. The first novelty consists in the restriction in choosing the reference image. Due to the demonstrated difference in backscattering between the snow free terrain and the dry snow, the latter is considered as reference.

Single snow layer backscattering is simulated by applying fundamental scattering theories: Integral Equation Model, Quasi Crystalline Approximation and Quasi Crystalline Approximation with Coherent Potentials. Qualitative conclusions concerning the interaction between the two snow types and the electromagnetic waves are drawn [10]. Additionally, some conclusions referring to the wet snow backscattering are confirmed through *in situ* measurements, validating the proposed simulator. Consequently, it is shown that the ratio between the wet and dry snow backscattering coefficients is significantly sensitive to the value of the local incidence angle (LIA), therefore requiring the use of a variable threshold (function of the LIA).

Further, the speckle noise statistics [11], [12], [13], [14], [15] is introduced through the local estimation of the backscattering coefficients ratio probability. This allows additional enhancement of the discrimination accuracy, which is illustrated through the matching of the independently obtained HH and VV maps. The validation is performed by comparing snow maps obtained using TerraSAR-X data with interpolated temperature map.

The paper is organized as follows. In Section II, we briefly introduce the proposed snow backscattering simulator (SBS)

followed by the simulation results and by the comparison with *in situ* ground based radar measurements. This section contains the qualitative conclusions concerning dry and wet snow backscattering. Section III is the core of the article, containing the description of the wet snow detection algorithm. In Section IV, we present the results obtained with two TerraSAR-X dual-pol stripmap images acquired in the French Alps. This section as well provides the method validation, while Section VI concludes this article.

II. Snow backscattering analysis

On one side, dry snow is characterized by a dielectric constant depending on the ice volume fraction, only. In this case, the dielectric constant is real, indicating the absence of medium dielectric losses [4], [16]. One can notice that a general consensus has not yet been achieved in the scientific community: the work of Matzler et al. [17], [18] may indicate a complex dielectric constant. We have adopted the former assumption [4], [16] by neglecting the imaginary part.

On the other side, the wet snow dielectric constant is a complex quantity with the imaginary part reflecting the presence of medium absorption losses. It is also function of the ice volume fraction, as well as of the wetness and the operating frequency [4], [19].

In terms of scattering theory, the extinction (absorption and scattering) properties of the two snow volume types require different approaches in volume modeling. The model we use for dry snow is based on the multiple scattering assumption: Quasi Crystalline Approximation (QCA) through the Dense Media Radiative Transfer (DMRT), taking thus into account the scattered waves influence on the other particles. Furthermore, it assumes waves coherence and it stays valid even in the case of a media more dense than the dry snow [20], [21]. Note that the extinction losses are reduced to the scattering phenomena only by neglecting the electromagnetic absorption of the ice particles (real ice dielectric constant). We assume the effective shape of the particles to be spherical.

The wet snow medium reveals a significant spatial variation of dielectric permittivity [20], [21]. Such an important difference in dielectric properties (between the host medium and the scattering particles) requires applying a modified QCA theory. Hence the selected QCA with Coherent Potentials (QCA-CP) assumes that the coherent wave interacts with the new average medium rather than the host one. The water inclusions are introduced by means of mixed ice-water spherical particles [22] with a radius determined by the wetness. Due to non negligible wet snow absorption we introduce the albedo coefficient, also [23].

[Figure 1 about here.]

The total backscattering coefficient σ_0 of a snow pack (distributed target) is expressed as the sum of four backscattering coefficients, corresponding to the following components [24], [25] (Fig. 1):

1) Snow pack surface component (σ_s),
2) Underlying ground surface component (σ_{gr}),
3) Snow volume component (σ_v),
4) Ground-volume interaction component (σ_{gv}),

$$\sigma_0 = \sigma_s + \sigma_{gr} + \sigma_v + \sigma_{gv}. \tag{1}$$

Surface backscattering is simulated using the Integral Equation Model (IEM-B) by assuming an isotropically exponentially correlated surface (introduced through the surface spectra) [24].

The output result is the angular distribution of the backscattering coefficient for different values of snow pack parameters. The incidence angle ranges from 0° up to 70°.

[Table 1 about here.]

Table 1 shows the input parameters for the snow backscattering simulations. The selected values are set either according to [4], [26] (for the ice and water dielectric permittivities), or according to the local *in situ* measurements[1][2]. The surface Root Mean Square (RMS) height represents a potential exception: a 12 mm ground RMS height is not actually corresponding to the terrain roughness. The value of this parameter is strictly imposed by the IEM-B model limitations and by the constrain of using same surface properties for each frequency band (limitting value at 10 GHz) [24].

We summarize in the sequel our conclusions with respect to the dry/wet snow backscattering behavior. Despite the fact that the detection strategy introduced in Section III is designed with X band SAR images, the necessity to demonstrate the particularities of the snow target backscattering in this band, and the potential of broader frequency coverage, imposed the comparative study with respect to C and L bands.

A. Dry snow

According to previous simulation results [9], the dominant component of dry snow backscattering is the underlying ground component for all three frequency bands. This is particularly true at L band, because both snow pack surface and volume component are increasing with the increase in frequency. In general, dry snow backscattering can be considered as not significantly sensitive to the depth of the layer, but fairly sensitive to the snow density.

[Figure 2 about here.]

Fig. 2 illustrates the rise in backscattering (underlying ground component) at L band with the increase of snow density. Firstly noticed by Shi and Dozier, this phenomenon was explained by the fact that the density dominantly affects backscattering through the change of the air-snow interface refraction angle and the change of the wavelength in the snow medium [1]. The near correspondence between [1] and our qualitative conclusions (with slightly different input parameters) validates the simulation framework proposed in this paper.

At C band, and by assuming the same roughness parameters, the former effect is not present any more: density increase causes decrease of backscattering (Fig. 2). This is because density dominantly affects backscattering through the change in ground-snow dielectric contrast.

The underlying ground component remains dominant at X band. Fig. 2 shows the same backscattering behavior with respect to the density change as for the C band. However, the sensitivity is significantly increased. On one side, the impact of the

[1] ©*Électricité de France (EDF).*
[2] ©*Météo-France.*

change in the ground-snow dielectric contrast is independent of frequency. On the other side, the ground incident wavelength and the change in ground incident angle are inducing the effect opposite to the one characteristic for the L band.

B. Wet snow

The dominant backscattering component of wet snow is the snow pack surface component [9]. This causes high sensitivity of the wet snow backscattering on wetness change. Therefore, the increased wetness, reflected by an increase in wet snow dielectric constant, leads to stronger total backscattering.

Nevertheless, the initial assumption which justifies the change detection approach is not compromised. The difference in backscattering intensity with respect to the corresponding dry snow is maintained, due to the difference in both the dielectric constant and the roughness properties, between the upper wet snow layer and the underlying ground. This remains true for a wide range of wetness values [19].

[Figure 3 about here.]

On one side, higher operating frequency would suggest stronger snow-pack surface backscattering. On the other side, the increase in frequency is causing the decrease of the wet snow dielectric constant [4]. According to our simulator, the backscattering decrease due to the later effect exceeds the former increasing phenomena [27]. This indicates the reduced share of snow pack surface component in total backscattering at higher frequencies.

[Figure 4 about here.]

1) "In situ" measurements: This paragraph deals with the analysis of X-band ground based radar signals (VV polarization channel) acquired on the 23rd of April 2013, in the Grand Rousse region of the French Alpes. Two sets of measurements were performed over the same spot (same surface parameters) at 4 hour interval. The first set of range profiles was acquired in the morning, while the second acquisition took place in the afternoon, allowing snow wetness variation in the upper snow layer due to the sunny weather conditions. The parameters of the upper snow layer which characterize the snow pack surface backscattering component were carefully measured (see Table 2).

[Table 2 about here.]

The backscattering coefficients for different local incidence angles are derived from the corresponding ground range profiles. Fig. 3 illustrates the comparison between the measured and the scaled simulated backscattering sensitivity on wetness of the upper layer. One can notice that the backscattering intensity is directly proportional to the wetness of the upper layer. This result, although not qualitatively consistent with the analysis in [28], confirms the wet snow pack surface backscattering component is indeed dominant.

In summary, the conclusions derived in this section point out unequivocally that the entire complexity of the snow backscattering should not be neglected in distinguishing between wet and dry snow covers. Moreover, simply assuming that less intense wet snow backscattering is only due to the electromagnetic absorption induced by water inclusions, can be misleading. This

is especially true at X band: the dominance of both the underlying ground component of dry snow and the snow pack surface component of wet snow backscattering, indicates that the expected backscattering difference should be treated as a function of the parameters determining surface backscattering. Therefore, it is necessary to introduce a variable threshold (rather than unique) for change detection.

III. The detection algorithm

In the proposed algorithm, a variable change detection threshold is introduced as a local function of the Local Incidence Angle (LIA) and a global function of the operating frequency. This step is justified by the significant sensitivity of the ratio between the wet and dry backscattering coefficients to the value of local incidence angles (Fig. 6) and by the fact that the operating frequency affects the change detection approach through the threshold value, exclusively.

Aside from those, the speckle noise statistics is used in the estimation procedure, making this method stochastic. It provides the wet snow probability map, which is transformed into the binary map based on the reliability of the variable threshold.

The wet snow detection algorithm (Fig. 4) is consisting of four principal parts.

A. Input data

The following data are required as input:

1) Winter SAR image (W), slant range geometry - image acquired during the winter season, when the dry snow assumption is fairly valid due to the air temperature at ground level;
2) Melting season SAR image (M), slant range geometry - image acquired at the end of the winter season, when the increase in the air temperature causes melting to occur;
3) Digital Elevation Model (DEM) and Sensor & Orbit parameters;
4) Terrain characteristics - approximate information about the terrain roughness and its dielectric properties,
5) Optical snow free terrain image - image acquired during the period when the type of the underlying ground can be observed.

According to our backscattering simulator results (averaged over different underlying ground dielectric constant and grain size values), the assumption that bare ground and dry snow backscattering difference is always smaller than -3 dB is not valid for the X band (Fig. 5). This implies that, at higher frequencies, the difference between bare ground and melting season backscattering coefficients, which is greater than 3 dB, does not unambiguously impose the wet snow presence. The results from Fig. 5 are questioning this assumption for C band. Therefore, the comparison is made directly between the dry snow cover image and the mixed dry/wet snow cover one in order to assure applicability in a wider range of frequencies.

[Figure 5 about here.]

B. SAR image processing

In this part, the input images are calibrated and corregistrated using the resampled SAR geometry intensity simulation. The slant range LIA is also derived.

[Figure 6 about here.]

C. Probability map

The backscattering simulator provides the variable threshold matrix T (Fig. 6), function of the local incidence angle for a given terrain *a priori* characteristics. These values are derived as the ratio of the simulated wet and dry snow backscattering results, averaged over different wet snow volumetric liquid water content, particle size, and underlying ground dielectric permitivity values (Table 1).

Assuming the gaussianity of the SAR clutter, the intensity over homogeneous regions can be modeled by Gamma probability density function, according to the fully developed speckle model [29]:

$$\mathcal{G}(\tau|\nu,\mu) = \frac{1}{\Gamma(\nu)}\left(\frac{\nu}{\mu}\right)^{\nu}\tau^{\nu-1}e^{-\frac{\nu x}{\mu}}, \tag{2}$$

with μ being the texture intensity mean, ν - shape factor providing deviation with respect to the corresponding Gaussian distribution and Γ - the Gamma function. If the intensity is expressed as $\frac{\mu}{\nu}X$, the random variable X follows chi-squared distribution $\chi^2(\nu)$ with ν degrees of freedom. The ratio of two chi-squared random variables, normalized with respect to the degrees of freedom, follows Fisher-Snedecor distribution $\mathcal{F}(\nu_1,\nu_2)$ [30]. This implies that the ratio of two Gamma random variables, having different shape factors but the same mean value is modeled using the Fisher-Snedecor distribution:

$$\mathcal{F}(r|k,\nu_1,\nu_2) = \frac{\Gamma(\nu_1+\nu_2)}{\Gamma(\nu_1)\Gamma(\nu_2)}\frac{\nu_1}{k\nu_2}\frac{(\frac{\nu_1 r}{k\nu_2})^{\nu_1-1}}{(1+\frac{\nu_1 r}{k\nu_2})^{\nu_1+\nu_2}}. \tag{3}$$

The proposed stochastic approach is exactly based on the probability estimation relaying on the previously elaborated assumption. The algorithm uses the boxcar neighborhood, coupled with approximate maximum likelihood estimator, in order to obtain local statistics for each of the areas in the image. Due to the poor performances of the Fisher-Snedecor MLE, the estimation is performed rather on the normalized ratio intensity (ξ) than the ratio intensity itself ($r = \mu\xi$).

If the ratio intensity (r) follows the Fisher-Snedecor distribution, the normalized ratio intensity (ξ) is modeled by Beta prime distribution:

$$\mathcal{B}'(\xi|\nu_1,\nu_2) = \frac{\Gamma(\nu_1+\nu_2)}{\Gamma(\nu_1)\Gamma(\nu_2)}\frac{\xi^{\nu_1-1}}{(1+\xi)^{\nu_1+\nu_2}}. \tag{4}$$

For each local neighborhood, we are deriving the mean value (μ), normalizing the texture locally and estimating ν_1 and ν_2 parameters. This way, we are able to define the probability density function ($\mathcal{B}'_{(i,j)}$) for every possible region in the image. By integrating the obtained PDF with respect to the normalized texture, we are getting the cumulative distribution function ($B'_{(i,j)}$) for the normalized threshold of the central pixel:

$$i_{out}(i,j) = B'_{(i,j)}\left(\frac{T(i,j)}{\mu(i,j)}\right) = \int_{-\infty}^{\frac{T(i,j)}{\mu(i,j)}}\mathcal{B}'_{(i,j)}(\xi)d\xi. \tag{5}$$

This value is the probability that the ratio is smaller or equal to the local threshold or exactly the wet snow probability.

[Figure 7 about here.]

D. Confidence level

The obtained wet snow probability map is transformed into the wet snow binary map by defining the confidence level C:

$$I_{out}(i,j) = \begin{cases} 1 & \text{if } i_{out}(i,j) \geq C, \\ 0 & \text{if } i_{out}(i,j) < C. \end{cases} \tag{6}$$

The confidence level value is related to the underlying terrain properties. Namely, the simulator generating the variable threshold is assuming the bare sol as the underlying ground. Any kind of model mismatch is decreasing the reliability of the computed variable threshold. In the final step, this effect can be compensated through the confidence level value: globally or locally, depending on the degree of the *a priori* know terrain characteristics.

Having the optical image of the targeted snow-free terrain among the input data, we are able to classify different distributed targets. We are locally assigning the confidence level which deviates from the full confidence (one) proportionally to the distance between the given class and the bare ground in the orthogonalized space of the given image (Fig. 8). This way we are accounting for the presence of low vegetation, forests, lakes and glaciers in the region of interest, compromising the validity of the derived threshold.

Otherwise, the global confidence level is estimated based on the overall validity of the assumed terrain characteristics, the ground dielectric constant particularly.

[Figure 8 about here.]

IV. Results and discussion

The proposed algorithm is illustrated by the results obtained using two X-band TerraSAR-X stripmap images (Fig. 7) acquired over the Grand Rousse massif near Grenoble, France:

- the winter image acquired on the 08th of February 2009 holding for the dry snow assumption according to the local meteorological data,
- the melting season image acquired on the 02nd of March 2009 in the presence of wet snow, according to the same source.

The local incidence angle map is computed using the Digital Terrain Model (Datum: WGS-84, UL Geo: $5°57'3.64''E, 45°24'15.21''N$) provided by the *Institut national de l'information géographique et forestière (IGN France)*.

For comparison, we provide in Fig. 8 several pairs of binary maps (HH and VV) derived using different change detection methods. The first set of images (a,e) present the results obtained by applying the variable threshold on the ratio of original input images. The following set (b,f) is derived by performing spatial speckle filtering on the input images before calculating the ratio of SAR intensities. The last two sets are the final outputs of our algorithm (before georeferencing): firstly by thresholding the

probability maps with a global value of confidence level, and secondly by using a predefined confidence level map for locally thresholding the probability. This map has been derived from an optical image (SPOT) acquired during the snow-free season.

The quantitative correspondence between the HH and VV maps, as it can be seen in Fig. 8, augments in case of the proposed stochastic approach.

The qualitative verification of the proposed method validity is performed using the local temperature measurements at the ground level. The measurements data, provided by the *Électricité de France (EDF)*, are related to the area of interest (Grand Rousse massif) at the same date (03 March 2009), meaning that comparison with the available SAR images was possible.

The procedure is based on the stated fact that wet snow presence is characteristic for the local ground temperature above $0°$C, while dry snow can be found below $0°$C. The temperature measurements are compared to the obtained wet snow probability maps (Fig. 9). The approximate matching between the high temperature regions and the high probability regions, two information sources which could be considered as independent, is pointing to the validity of the proposed method.

[Figure 9 about here.]

Using the matching percentage between the HH and the VV binary maps as a quantitative indicator (Fig. 8), the proposed method can be considered as an improvement in the wet snow detection. This is particularly true when using the locally predefined confidence level. The implicitly introduced spatial correlation between the wet snow areas, on one side, and the possibility to subtly account for the presence of different distributed targets underlying the snow layer by thresholding the obtained probability map, on the other side, bring the introduced stochastic approach superior with respect to conventional change detection approaches.

Note that the illustrated relation between the bare ground and dry snow backscattering (Fig. 5) indicates that the eventual presence of the bare ground in the melting season image cannot cause a false wet snow detection.

V. Conclusions

Based on fundamental scattering theories, the proposed backscattering simulator allowed us to demonstrate the different backscattering mechanisms of the dry and the wet snow cover. The detailed sensitivity analysis pointed out the dominance of the underlying ground backscattering component in case of dry snow and the dominance of snow pack surface component in case of wet snow. The later conclusion is confirmed by the performed *in situ* measurements. Rather than assuming the cause of the backscattering difference to be the absorption phenomena of the wet snow due to the water inclusions, we provided a detailed comparative description of the backscattering. It resulted in the conclusions that the difference occurs to be significantly dependent on the local incidence angle and the operating frequency. Consequently, we have proposed an improvement of the conventionally used wet snow detection method, by introducing a variable threshold given as function of the local incidence angle for each pixel and function of the operating frequency, also. This fact, as well as the choice of the winter image as the reference, allows application in wider frequency range. Instead of directly thresholding the ratio of multitemporal images, by considering the spatial correlation, we rather estimate the probability of the wet snow occurrence, making the algorithm stochastic.

Further refinements of the proposed detection method are going in two main directions. In the first, the other parameters significantly affecting surface backscattering (e.g. roughness and dielectric constant) would be also included as spatial variables in the threshold derivation. These parameters will be either retrieved by means of spaceborne remote sensing or by interpolating the local *in situ* measurements. Concerning the second direction, further work will mostly consist in adjusting the proposed method to polarimetric SAR input data [31]. The idea is to exploit the dual-pol images in the probability derivation, rather than just using them in the verification of the results.

ACKNOWLEDGMENT

The authors would like to thank to the *Électricité de France (EDF)* and the *Météo-France* for providing us the ground truth temperature data and other input parameters of interest, and to the *Institut national de l'information géographique et forestière (IGN France)* for the DEM. The SPOT optical image was provided by the ISIS 2011-593 contract, copyright CNES/Spot-Image.

REFERENCES

[1] J. Shi and J. Dozier, "Estimation of snow water equivalence using sir-c/x-sar, part i: Inferring snow density and subsurface properties," *IEEE Trans. Geosci. Remote Sens.*, vol. 38, no. 6, pp. 2465–2474, 2000.
[2] F. T. Ulaby and W. H. Stiles, "Microwave response of snow," *Advances in Space Research*, vol. 1, no. 10, pp. 131 – 149, 1981.
[3] H. Rott and C. Matzler, "Possibilities and limits of synthetic aperture radar for snow and glacier surveying," *Annals of Glaciology*, no. 9, pp. 195–199, 1987.
[4] W. G. Rees, *Remote Sensing of Snow and Ice*. Boca Raton, FL, USA: CRC Press, Taylor and Francis Group, 2006.
[5] F. T. Ulaby, W. H. Stiles, and M. AbdelRazik, "Snowcover influence on backscattering from terrain," *IEEE Trans. Geosci. Remote Sens.*, vol. GE-22, no. 2, pp. 126 –133, march 1984.
[6] H. Rott, "Thematic studies in alpine areas by means of polarimetric sar and optical imagery," *Advances in Space Research*, vol. 14, no. 3, pp. 217–226, 1994.
[7] H. Rott and T. Nagler, "Capabilities of ers-1 sar for snow and glacier monitoring in alpine areas," in *Proceedings of ERS-1 2nd symposium*, 1994, pp. 965–970.
[8] T. Nagler and H. Rott, "Retrieval of wet snow by means of multitemporal sar data," *IEEE Trans. Geosci. Remote Sens.*, vol. 38, no. 2, pp. 754–765, 2000.
[9] N. Besic, G. Vasile, J. Chanussot, S. Stankovic, J.-P. Ovarlez, G. d'Urso, D. Boldo, and J.-P. Dedieu, "Stochastically based wet snow mapping with sar data," in *Proc. IEEE International Geoscience and Remote Sensing Symposium (IGARSS'12)*, Munich, Germany, 2012, pp. 4859–4862.
[10] N. Besic, G. Vasile, J. Chanussot, S. Stankovic, J.-P. Dedieu, G. d'Urso, D. Boldo, and J.-P. Ovarlez, "Dry snow backscattering sensitivity on density change for swe estimation," in *Proc. IEEE International Geoscience and Remote Sensing Symposium (IGARSS'12)*, Munich, Germany, 2012, pp. 4418–4421.
[11] G. Vasile, I. Petillot, A. Julea, E. Trouvé, P. Bolon, L. Bombrun, M. Gay, T. Landes, P. Grussenmeyer, and J. M. Nicolas, "High resolution SAR interferometry: influence of local topography in the context of glacier monitoring," in *IEEE Geoscience and Remote Sensing Symposium, Denver, USA*, 2006, pp. 4008–4011.
[12] A. Julea, G. Vasile, I. Petillot, E. Trouvé, M. Gay, J. M. Nicolas, and P. Bolon, "Simulation of SAR images and radar coding of georeferenced information for temperate glacier monitoring," in *Proc. OPTIM, Brasov, Romania*, vol. 4, 2006, pp. 175–180.
[13] G. Vasile, F. Pascal, J. P. Ovarlez, P. Formont, and M. Gay, "Optimal parameter estimation in heterogeneous clutter for high resolution polarimetric SAR data," *IEEE Geoscience and Remote Sensing Letters*, vol. 8, no. 6, pp. 1046–1050, 2011.
[14] A. Anghel, G. Vasile, C. Cacoveanu, C. Ioana, and S. Ciochina, "Short-range wideband FMCW radar for millimetric displacement measurements," *IEEE Transactions on Geoscience and Remote Sensing*, vol. 52, no. 9, pp. 5633–5642, 2014.
[15] N. Besic, G. Vasile, J. P. Dedieu, J. Chanussot, and S. Stankovic, "Stochastic approach in wet snow detection using multitemporal SAR data," *IEEE Geoscience and Remote Sensing Letters*, vol. 12, no. 2, pp. 244–248, 2015.
[16] M. Hallikainen, F. Ulaby, and M. Abdelrazik, "Dielectric properties of snow in the 3 to 37 ghz range," *Antennas and Propagation, IEEE Transactions on*, vol. 34, no. 11, pp. 1329–1340, 1986.
[17] C. Matzler, *Solar System Ices*. Springer Netherlands, 1998, ch. Microwave properties of ice and snow, pp. 241–257.
[18] C. Matzler and U. Wegmuller, "Dielectric properties of freshwater ice at microwave frequencies," *Journal of Physics D.: Applied Physics*, vol. 20, pp. 1623–1630, 1987.
[19] M. T. Hallikainen and D. P. Winebrenner, *Microwave Remote Sensing of Sea Ice*. American Geophysical Union, 1992, ch. The physical basis for sea ice remote sensing.
[20] L. Tsang, J. Kong, K. Ding, and C. Ao, *Scattering of Electromagnetic Waves, Vol. 2: Numerical Simulations*. Wiley Interscience, 2001.
[21] L. Tsang, J. Kong, and K. Ding, *Scattering of Electromagnetic Waves, Vol. 1:Theory and Applications*. Wiley Interscience, 2000.
[22] N. Longepe, S. Allain, L. Ferro-Famil, E. Pottier, and Y. Durand, "Snowpack characterization in mountainous regions using c-band sar data and a meteorological model," *IEEE Trans. Geosci. Remote Sens.*, vol. 47, no. 2, pp. 406–418, 2009.
[23] N. Longepe, "Snow remote sensing using spaceborne sar imagery at l- and c-bands," Ph.D. dissertation, University of Rennes I, Rennes, FR, 2008.
[24] A. K. Fung, D. Schutzer, and K. S. Chen, *Microwave Scattering and Emission Models for Users*. Norwood, MA, USA: Artech House, 2010.
[25] J. Shi and J. Dozier, "Estimation of snow water equivalence using sir-c/x-sar, part ii: Inferring snow depth and particle size," *IEEE Trans. Geosci. Remote Sens.*, vol. 38, no. 6, pp. 2475–2488, 2000.
[26] J. H. Jiang and D. L. Wu, "Ice and water permittivities for millimeter and sub-millimeter remote sensing applications," *Atmospheric Science Letters*, no. 5, pp. 146–151, 2004.
[27] N. Besic, G. Vasile, J. Chanussot, S. Stankovic, D. Boldo, and G. d'Urso, "Wet snow backscattering sensitivity on density change for swe estimation," in *Proc. IEEE International Geoscience and Remote Sensing Symposium (IGARSS'13)*, Melbourne, Australia, 2013.
[28] A. N. Arslan, M. T. Hallikainen, and J. T. Pulliainen, "Investigating of snow wetness parameter using a two-phase backscattering model," *IEEE Trans. Geosci. Remote Sens.*, vol. 43, no. 8, pp. 1827–1833, 2005.

[29] J. W. Goodman, “Some fundamental properties of speckle,” *J. Opt. Soc. Amer.*, vol. 53, no. 11, pp. 1145–1149, 1976.
[30] L. Bombrun, G. Vasile, M. Gay, and F. Totir, “Hierarchical segmentation of polarimetric SAR images using heterogeneous clutter models,” *IEEE Trans. Geosci. Remote Sens.*, vol. 49, no. 2, pp. 726–737, 2011.
[31] A. Lessard-Fontaine, S. Allain-Bailhache, J.-P. Dedieu, and Y. Durand, “Multi-temporal dry and wet snow mapping in alpine context using polarimetric radarsat-2 time-series,” in *Proc. IEEE International Geoscience and Remote Sensing Symposium (IGARSS’12)*, Munich, Germany, 2012, pp. 1569–1571.

Input parameter	Dry snow	Wet snow
Snow density	180,190,200,210,220 kg/m^3	220,240,260,280,300 kg/m^3
Volumetric liquid water content	0 $\%$	3.6,5.6,7.6,9.6,11.6 (7,9,11,13) $\%$
Snow depth	2 m	
Frequency	1.5 (L), 6 (C), 10 (X) GHz	
Particle equivalent radius	225 (121,169,225,289,361) μm	
Ice dielectric constant	3.15	
Water dielectric constant	$80 + j50$	
Snow RMS height	10 mm	
Snow correlation length	50 mm	
Ground dielectric constant	6 (5,5.5,6,6.5,7)	
Ground RMS height	12 mm	
Ground correlation length	50 mm	

TABLE I: Input parameters for the snow backscattering simulations: values in brackets are used for computing the variable threshold (median values for particle equivalent radius and ground dielectric constant are employed in Section II for the snow backscattering analysis).

table

Parameter	Sample I	Sample II
Acquisition time	11h00	15h00
Snow dielectric constant	2.94	4.39
Volumetric liquid water content	06.8 $\%$	16.00 $\%$
Snow density	175 kg/m^3	250 kg/m^3
Snow depth	2.15 m	2.15 m

TABLE II: In situ measurements: snow parameters.

table

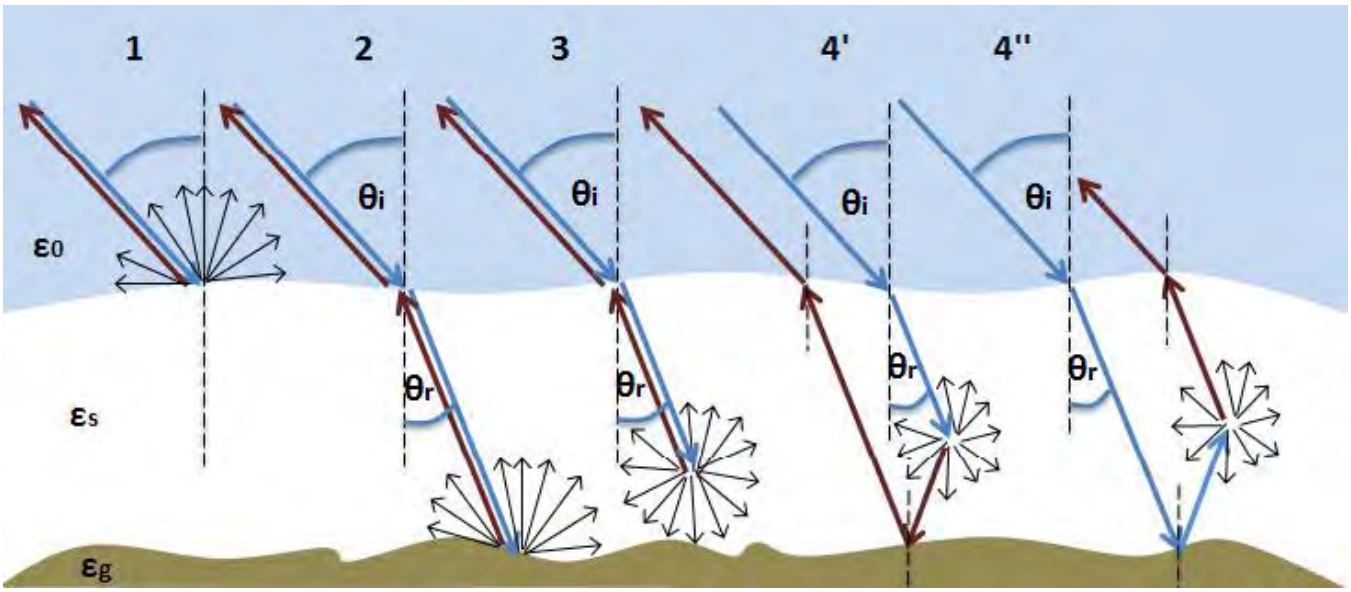

Fig. 1: Snow pack backscattering mechanism

figure

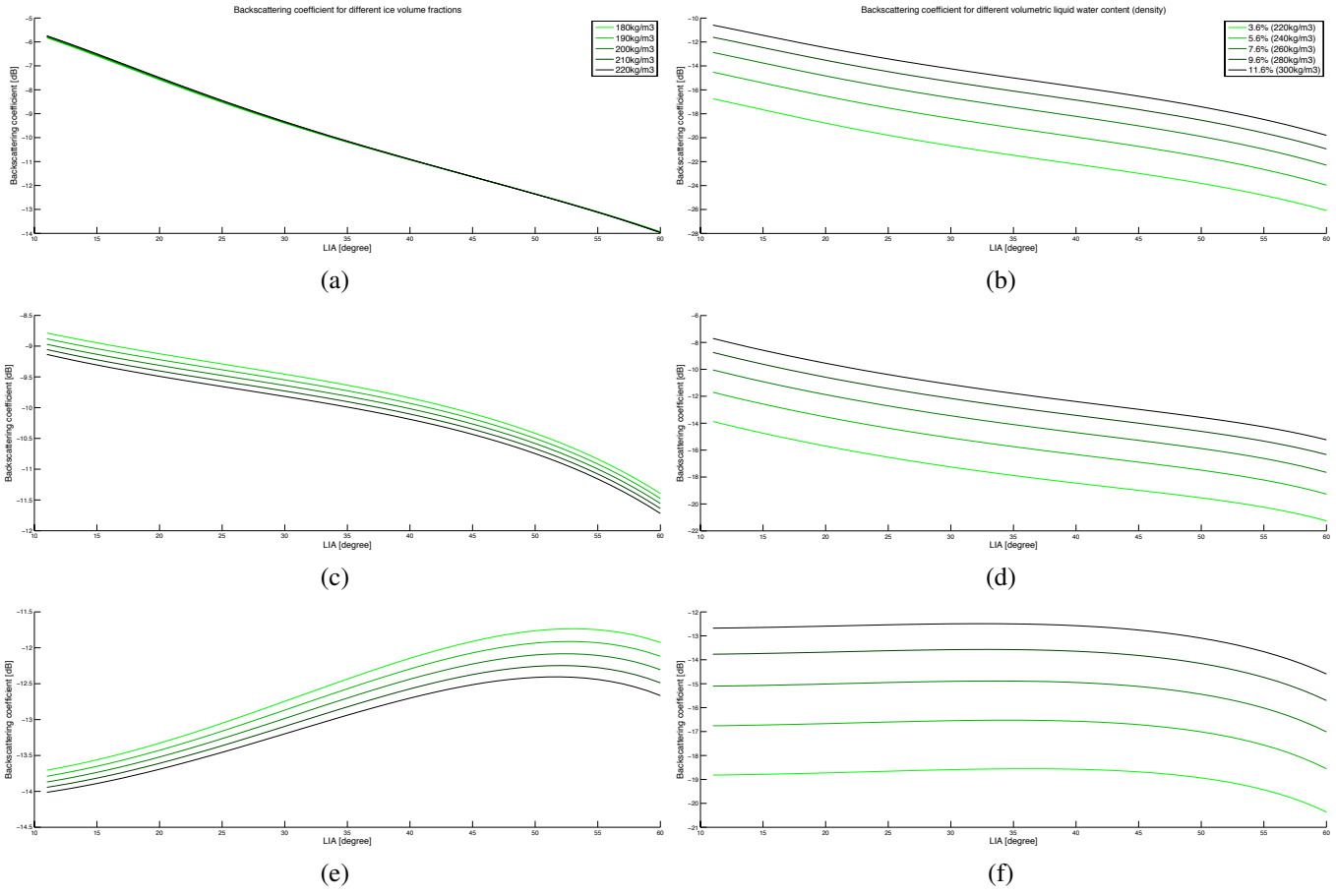

Fig. 2: Snow backscattering sensitivity on density change (VV polarisation channel): (a) dry snow, L band; (b) wet snow, L band; (c) dry snow, C band; (d) wet snow, C band; (e) dry snow, X band; (f) wet snow, X band.

figure

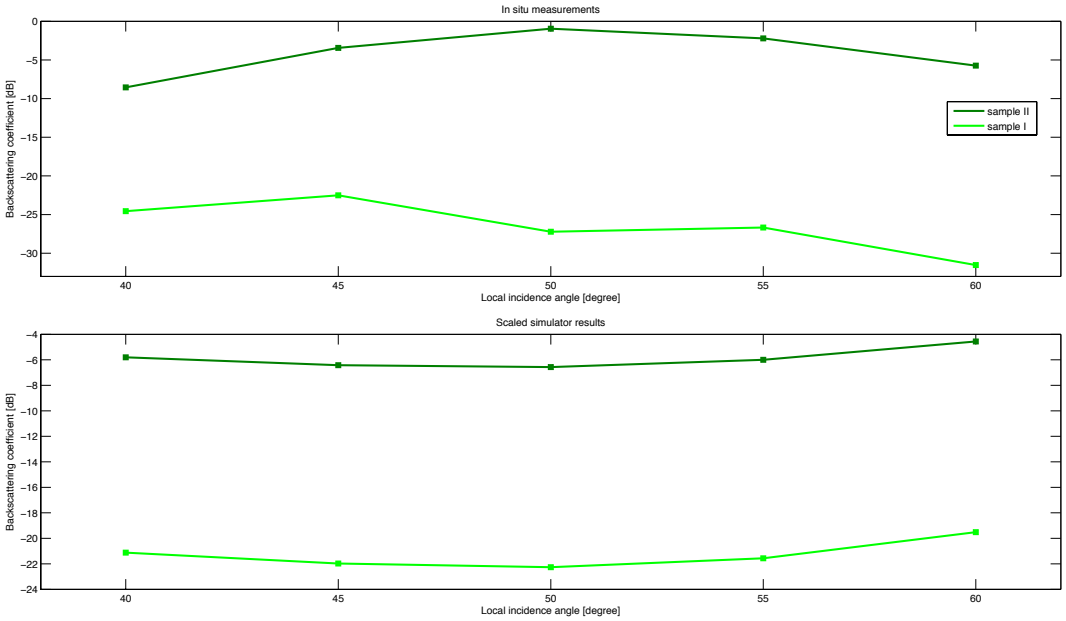

Fig. 3: Ground based X-band radar *in situ* measurements compared to simulation results.

figure

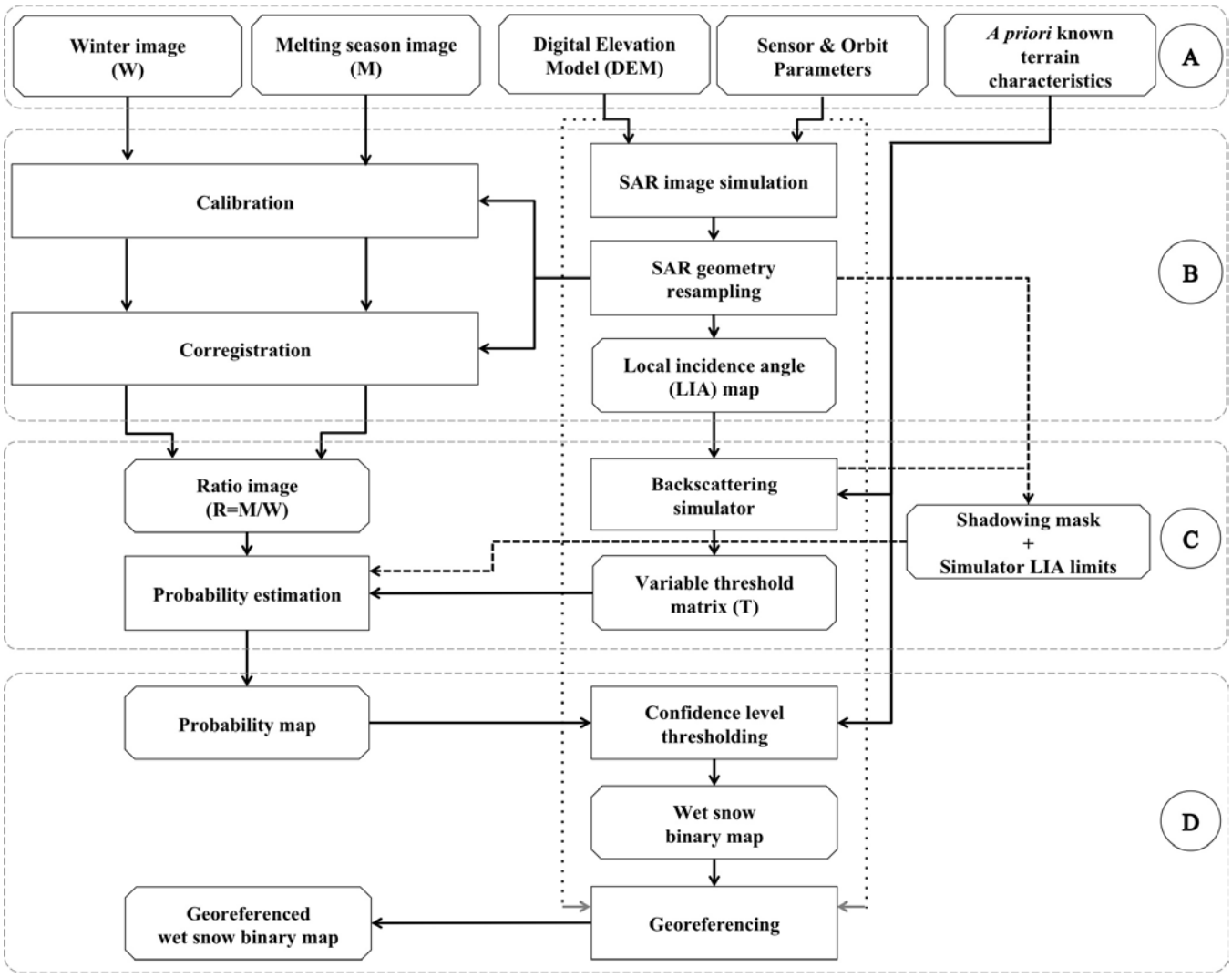

Fig. 4: Mapping algorithm

figure

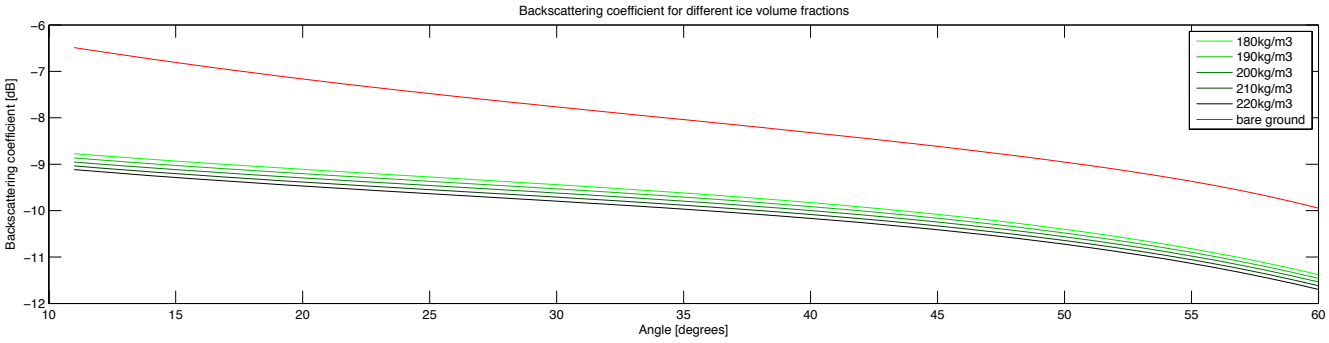

(a)

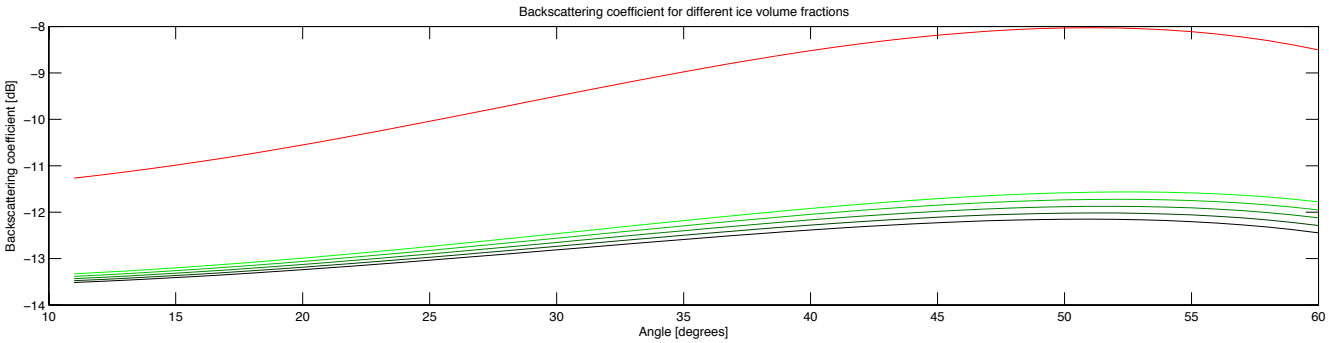

(b)

Fig. 5: Bare ground (red) backscattering and dry snow backscattering for different densities (green): (a) C band; (b) X band. figure

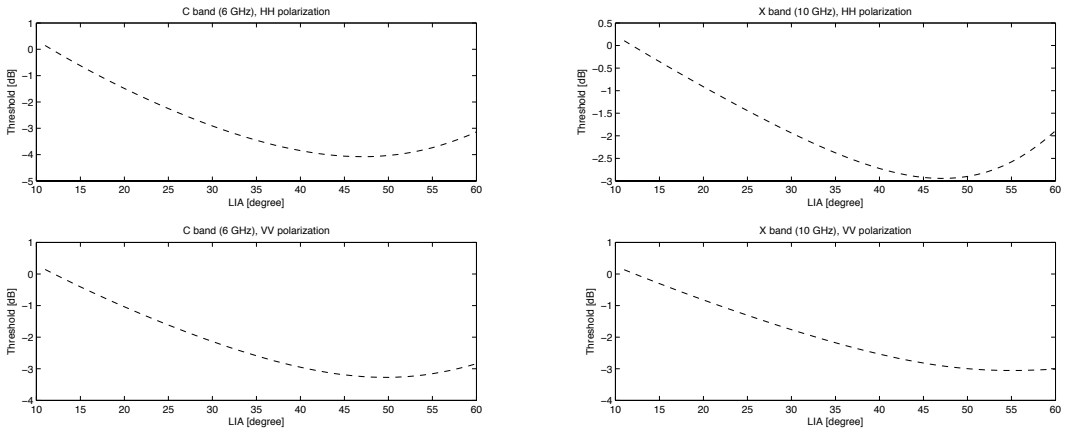

Fig. 6: Variable thresholds function of the LIA.

figure

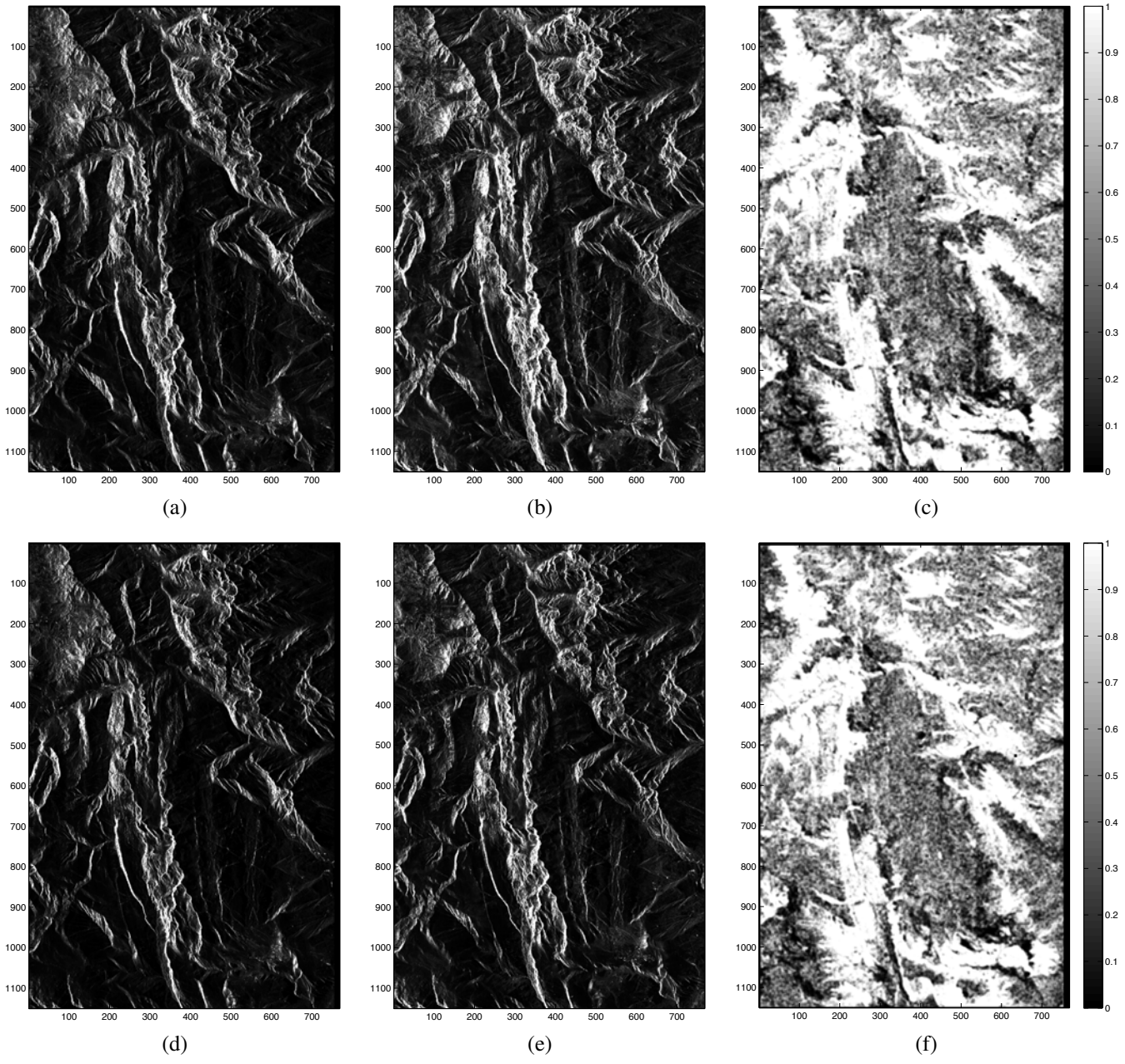

Fig. 7: TerraSAR-X, Grand Rousse, France, 1150x768 pixels: (a) HH slant range SAR image acquired on 08/02/2009; (b) HH slant range SAR image acquired on 02/03/2009; (c) HH slant range probability map; (d) VV slant range SAR image acquired on 08/02/2009; (e) VV slant range SAR image acquired on 02/03/2009; (f) VV slant range probability map.

figure

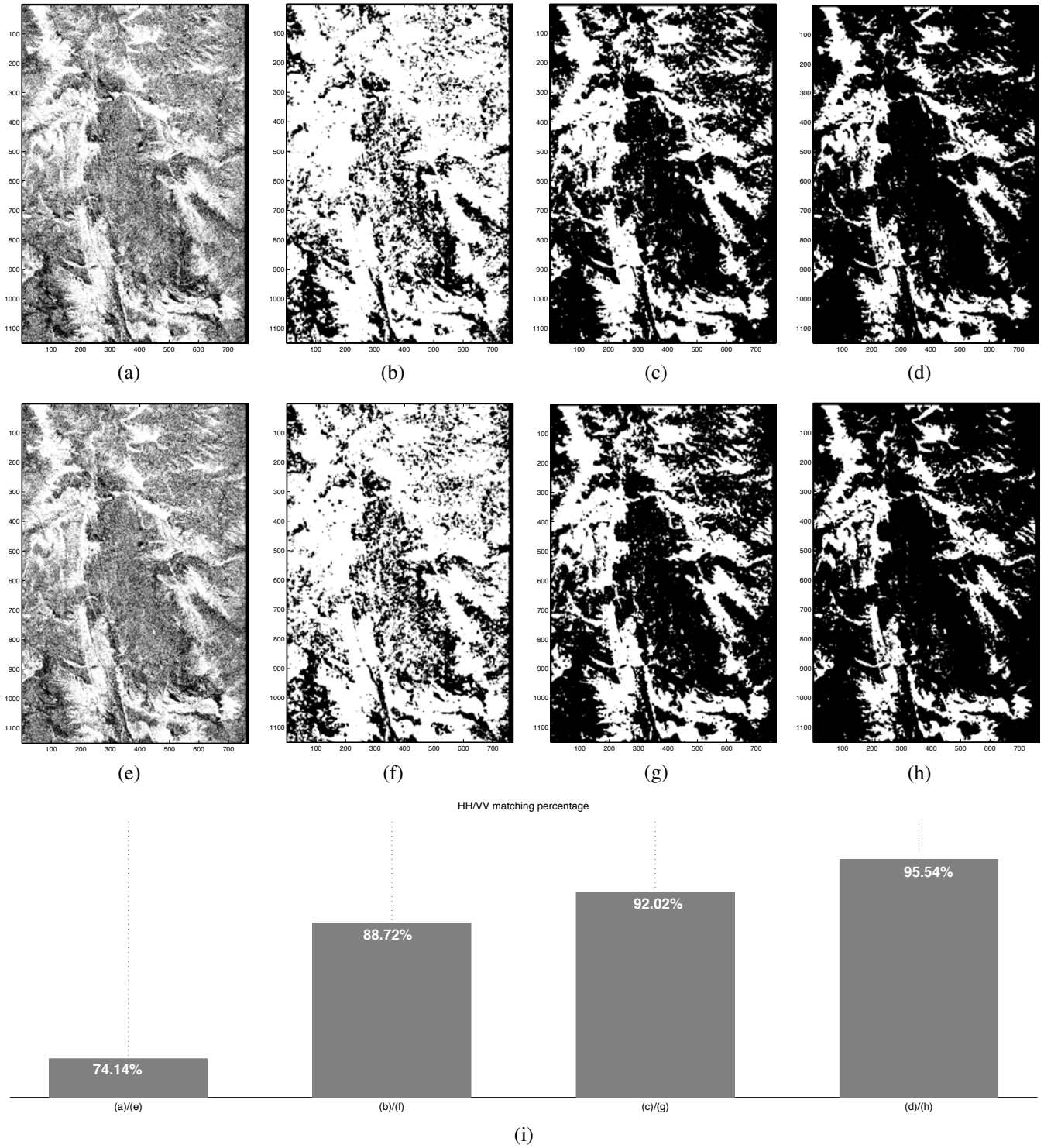

Fig. 8: The final wet snow binary maps comparison: binary map obtained after thresholding the ratio of input images (a) HH (e) VV; binary map obtained after thresholding the ratio of speckle (spatially) filtered input images (b) HH (f) VV; binary map obtained after thresholding the probability map with 75% confidence level (c) HH (g) VV;binary map obtained after thresholding the probability map with confidence level map derived from SPOT image (Path Row 051-259) acquired on 13/09/2011 (d) HH (h) VV; HH/VV matching percentage (i).

figure

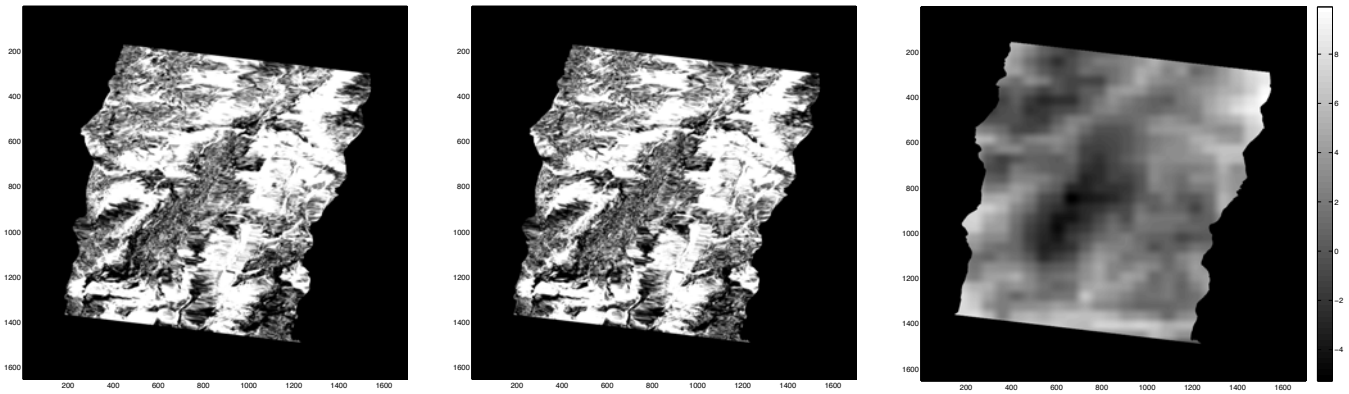

(a) (b) (c)

Fig. 9: Comparison with interpolated ground level temperature measurements: (a) georeferenced HH wet snow probability map; (b) georeferenced VV wet snow probability map; (c) georeferenced interpolated ground level temperature map [C°]. figure